Technical Paper

Alfred Strauss*
Saeed Karimi
Fritz Kopf
Catalin Capraru
Konrad Bergmeister

DOI: 10.1002/suco.201500019

Monitoring-based performance assessment of rail-bridge interaction based on structural reliability

For today's railways, the continuous welded rail, which enhances driving dynamics and comfort for passengers, is often the construction method of choice. However, bridges and viaducts, which can be seen as singularities in the railway substructure, still pose a few unsolved problems; the bridge structure deforms under the impacts of thermal variation, creep, shrinkage, train passage and braking. The track-bridge interaction is an important parameter in railway bridge design. Measurement campaigns and research projects have been performed to investigate the interaction process and learn how to predict longitudinal forces in the rail and the concrete slab track. For the construction of long bridges on high-speed railway lines, new computational tools, monitoring systems and enhanced verification methods for tolerable rail stresses on bridges had to be developed. In order to take the modified stiffness conditions and recent findings on rail resistance into account, the verification schemes and safety concepts based on monitoring data have to be revised and performance-based methods need to be developed. The target of this article is to present monitoring- and reliability-based assessment methods for the concrete structure-rail interaction using monitoring and non-linear analysis techniques.

Keywords: monitoring systems, non-linear modelling techniques, reliability assessment methods

1 Introduction

The track system in a railway infrastructure is a heavily loaded multi-component system whose individual components have to meet challenging demands while being subjected to great stresses. This circumstance leads to the unavoidable requirement of optimum coordination between the properties of the components. The components in the overall system, which consists of track and substructure with their planum and frost protection layers, are therefore constantly in a state of interaction. A continuous welded rail (CWR) meets the requirements of a modern railway infrastructure as far as possible. It facilitates passenger comfort and ride stability while at the same time reducing noise emissions. It also enables a very dynamic increase in train speeds and mitigates the stresses on track, substructure and vehicles according to current needs, see Fig. 1.

In the case of Austrian Federal Railways (ÖBB), the manufacture of CWR as well as the welding of track switches is regulated by [2]. This technical standard specifies and describes – for ballasted tracks as well as slab tracks – general requirements and specific characteristics regarding sleeper spacing, sleeper type related to track radii, gravel grain sizes, rigidity of the substructure, presence of engineering structures, neutral temperature of rails, tensioning and relaxation of rails, etc. Railway bridges are coupled to CWR via the ballast bed in the case of ballasted tracks and via the rail fastening system in the case of slab tracks. The longitudinal deformations in the bridge support structure mobilize a so-called shear flow between support structure and track panel and thus cause movements of the rails. An essential parameter for quantifying the effects of the interaction between rail and substructure is the free expansion length of the bridge, defined as the distance between the thermal reference point and the flexible end point of the support structure. The additional rail tensions occurring in continuously welded tracks can be limited either by reducing the free extension length or by fitting an expansion device as shown in Fig 2.

A further factor frequently addressed is to consider the thermal expansion factor of the bridges as a variable, which can be approached by probabilistic processes. Of course, the thermal expansion coefficient is independent of any circumstance or temperature variation, but it allows short-term temperature variations to be described which have a lesser effect than seasonal ones. A variable thermal expansion factor approach implies that surface temperature differs from inside temperature of the structure, and designers should not use the outside temperature variations when assessing rail stresses or deformations. This paper pursues an equivalent effective expansion coefficient approach in order to grasp the uncertainties of rail stresses or deformations associated with the effective temperature.

It should be noted, however, that expansion devices are dominant cost-increasing factors with respect to the life cycle cost (LCC) considerations of railway infrastructure systems and should be avoided whenever possible. Owing to this fact, extensive research activities associated with CWR and expansion devices are ongoing. For instance, the term "elastic reservoir" was introduced in [3] which addresses the continuous work on non-linear track-

* Corresponding author: alfred.strauss@boku.ac.at

Submitted for review: 4 February 2015
Revised: 15 May 2015
Accepted for publication: 11 June 2015

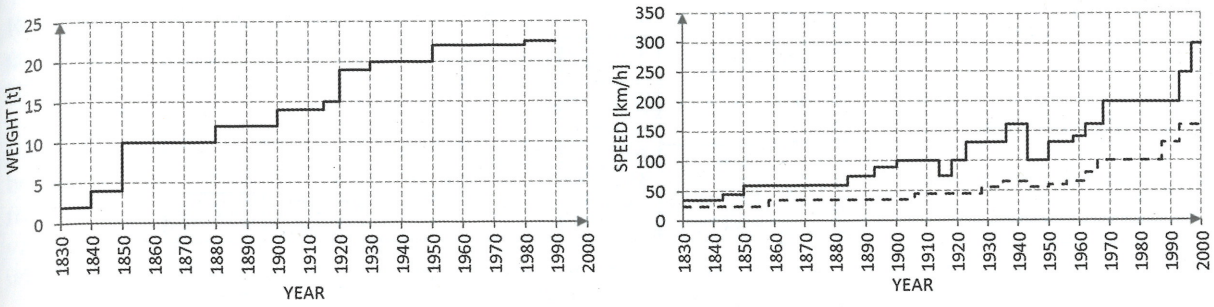

Fig. 1. Evolution of wheel set loads and speeds [1]

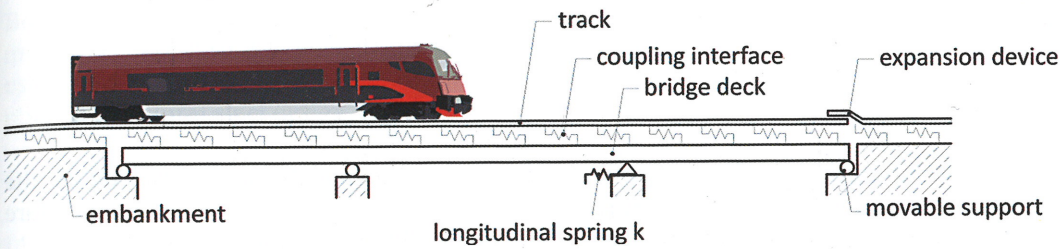

Fig. 2. Track/structure system model

Fig. 3. Instabilities in track position, track deformations, track warping, construction and expansion

bridge interaction [4], [5] intensified by the use of the available capacity on the system. In particular, the elastic capacity is characterized by: the capacity provided by the system to remain in an elastic condition due to actual loading. More details can be found in [6]. These research projects, among others, must be seen as very important owing to the fact that the introduction of expansion devices (see Fig. 2, right side) also leads to uneven vehicle passage caused by discontinuities in the track and hence has a bad effect on LCC optimization strategies while reducing the service life. This ultimately results in increases in the frequency and, consequently, the cost of maintenance measures.

In view of the design method (structural system, type and arrangement of bearings, etc.) and the attendant construction costs, limiting the free extension length has great potential for cost leverage. The acceptable free extension lengths are determined by code provisions and associated mechanical laws. For instance, EN 1991-2 [7], which is based on recommendations by the International Union of Railways UIC 774-3E 2, describes the laws of displacement resistance in tracks as a type of bilinear behaviour. The actual resistance values are characterized for both loaded and unloaded track as shown in Fig. 4a. The resistance values depend, on the one hand, on both the track-specific parameters and the track forms and, on the other, are significantly influenced by railway operation characteristics (magnitude and frequency of load, dynamic excitation of bridge support structure, etc.), weather conditions and the general maintenance conditions of the track system. Reinforced concrete has been used for the vast majority of bridge structures within the ÖBB Infra AG rail network (see Fig. 4b – bridge structures within the ÖBB Infrastruktur AG rail network).

Previous research, especially on the restriction of longitudinal stresses in CWR in order to ensure safety and stability (see Fig. 3a), is presented in [8], [9] and [10]. The coupling interface, which couples the elements of bridge and rail, plays an essential role; its presence enables the rail and the bridge to interact. As mentioned previously, to provide a convenient computational effort, the codes, such as EC-1 [7], present the non-linear stiffness law as the relationship between resistance and displacement, described by bilinear functions. The aim is to evaluate the force equilibrium of the system in the transitional situation by means of the change in the mechanical properties of the coupling in-

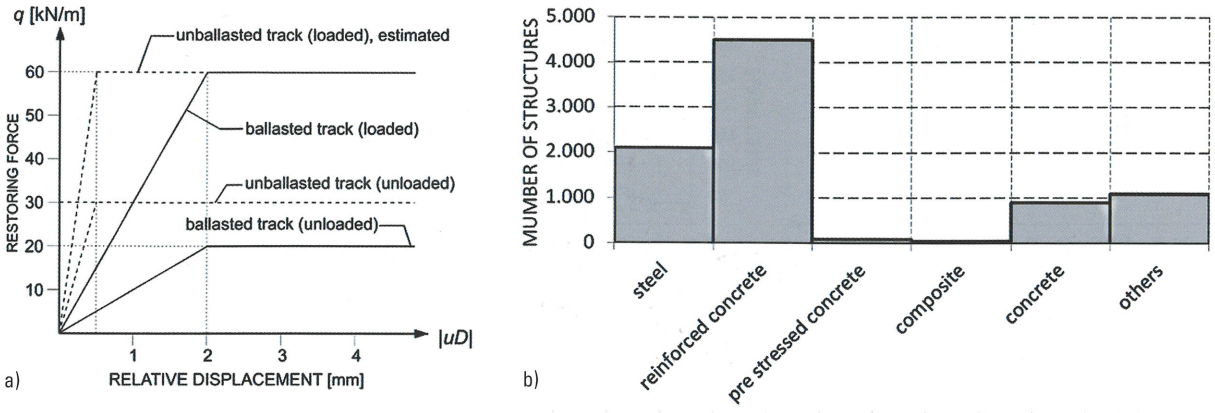

Fig. 4. a) Law of displacement resistance, b) bridge structures in the existing grid of Austrian Federal Railways within ÖBB Infrastruktur AG (source: ÖBB Infrastruktur AG)

terface between track and bridge deck. Although this effect is a clear consequence of the stiffness law, the phenomenon has not been mentioned in the codes to date. In this context, the longitudinal force is caused by temperature changes, bending, braking and accelerating. In accordance with the codes [7], the system is treated separately for each of the loads in a non-linear manner, and the total stress is then determined by summing up the individual results linearly. Fig. 5 illustrates these non-linear effects for different temperature load levels.

This procedure, however, is not in accordance with the non-linear character of the system. The current method – namely, treating the load combination as a linear sum – produces a larger stress value than would be the case when treating it in a non-linear manner. In fact, it leads to a result that lies on the safe side, and in some cases it leads to the unwelcome requirement of having to insert an expansion device at the free end of the bridge, as shown in Fig. 2. The aim of this article is to present monitoring- and reliability-based assessment methods, considering the non-linear character of the system, in order to describe and verify longitudinal rail stresses. This is essential for the safety and stability of the concrete bridge-rail track interaction. In particular, the objectives of this research have been to use observations from monitoring systems and laboratory studies of the longitudinal and shear resistance of the rail structure interaction for the calibration of non-linear finite element models and, consequently, the verification of the rail stresses caused by temperature changes in the rail and the structure.

2 Available stress capacity resistance

In general, additional stresses in CWR on a bridge should not exceed the admissible stress capacity as defined in DIN-Fb 101 [11] as follows:

- Tension stress threshold $\sigma_{tension} = 112$ N/mm^2 if bending is considered as load case.
- Tension stress threshold $\sigma_{tension} = 92$ N/mm^2 if bending is neglected.
- Compression threshold for a buckling ballasted track $\sigma_{compression} = 72$ N/mm^2.
- Compression threshold for a slab track $\sigma_{compression} = 92$ N/mm^2.

The admissible stresses above are based on the total available rail stress $\sigma_{safe} = 470$ N/mm^2 having to be reduced by:

- Residual stress due to production $\sigma_E = 80$ N/mm^2.
- Bending tensile stress due to wheel load $\sigma_Q = 158$ N/mm^2.
- Stress resulting from a temperature change in the rail $\sigma_T = E \cdot \alpha \cdot \Delta T = 120$ N/mm^2 assuming an elasticity modulus $E = 2.1 \cdot 10^5$ N/mm^2, a temperature difference $\Delta T = 50$ K and thermal coefficient $\alpha_T = 1.15 \cdot 10^{-5}$.

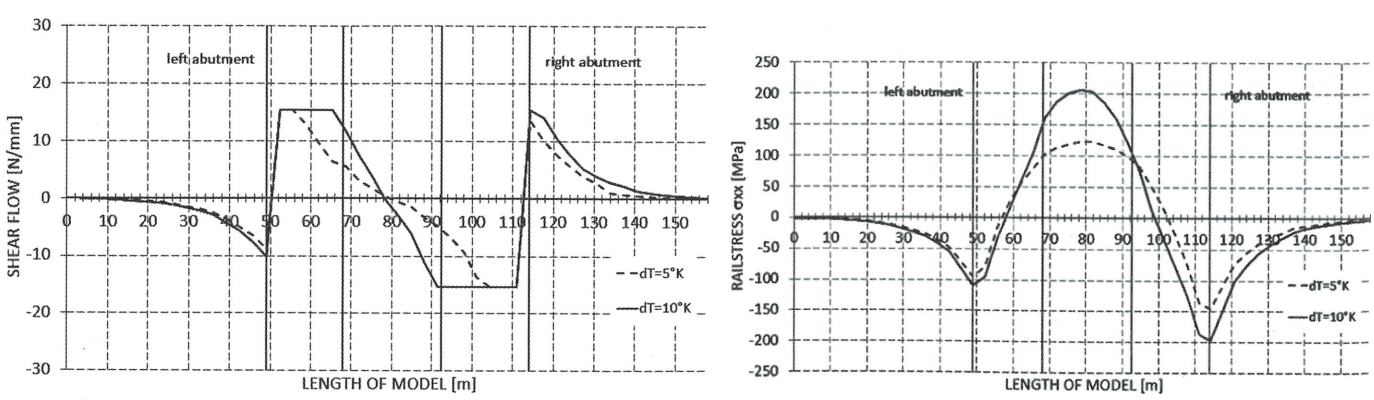

Fig. 5. Rail and bridge condition profiles for different structure temperatures of the L110 bridge. (See Fig. 6 for structural scheme and description of monitoring system.)

Reducing the safe rail stress σ_{safe} yields an admissible margin for the increase in rail stress due to the track-bridge interaction $\sigma_{tension} = (470 - 80 - 158 - 120) = 112$ N/mm^2.

In accordance with EC-1 [7] as well as DIN-Fb101 [11] and UIC774 [12], the use of expansion devices should be considered where additional stresses resulting from track-bridge interaction are larger than the permissible values. DIN-Fb101 [11] uses the classical safety concept where the safety is determined by a global safety factor:

$$S_{safe} = \frac{R}{\nu} \tag{1}$$

Both available strength S_{safe} and resistance R are deterministic. This classical deterministic safety concept is still used today. A more modern safety concept is already applied in structural steel design, e.g. DIN 18800 [13]:

$$F_d = F_c \cdot \gamma_F \tag{2}$$

In the authors' research, the reliability- or performance-based assessment approach has been applied in order to incorporate the essential information from the monitoring systems. In addition, with respect to safety against exceeding predefined rail stress thresholds, an elastic reservoir or capacity approach should also be considered.

3 Reliability assessment using monitoring information

MAGIT, the "monitoring-based analysis of track structures interaction" research project, commissioned monitoring campaigns on three bridges for recording the rail structure interaction. This section provides an overview of the reliability approach that has been used to assess the monitoring results and the following section presents the monitoring results and monitoring systems of the bridge investigated – over the L110 road. The following reliability-based methods served as a basis for the assessment of the aforementioned advanced monitoring concepts and their results. In general, two basic methods, FORM and SORM, are used to estimate the structural reliability. It was verified that the reliability analysis of FORM for linear and sometimes non-linear conditions provides an excellent approximation. The design of any structure requires that its resistance R is greater than the load effect Q [14]. The reliability index is defined as

$$\beta = (\mu_R - \mu_Q)/(\sigma^2_R + \sigma^2_Q)^{1/2} \tag{3}$$

where μ_R and μ_Q are the mean resistance and mean load effect respectively, and σ_R and σ_Q the standard deviations of the resistance and the load effect respectively. If the resistance R and the load effect Q are normally distributed, the probability of failure can be determined as

$$P_f = \Phi(-\beta) \tag{4}$$

where Φ is the standard normal probability function. The calculation of the reliability index β is a constrained optimization problem of finding the nearest point on the limit state surface in the standard normal space [15]. Using this optimization process, RELSYS [16] computes the reliability index and the associated probability of failure for non-deterministic systems under random loads.

4 Reliability method applied to sensor readings according to Frangopol et al., [14]

The monitoring of any structure requires that its resistance R is greater than the monitored load effect M (e.g. rail stresses or structural movements). This requirement (i.e. $R > M$), assuming normal distributions for R and M, can be expressed as

$$g(\mathbf{X}) = R - M > 0 \tag{5}$$

The reliability index is given as

$$\beta = (\mu_R - \mu_M)/(\sigma^2_R + \sigma^2_M)^{1/2} \tag{6}$$

where μ_R and μ_M are the mean resistance and mean monitored load effect respectively, and σ_R and σ_M the standard deviations of the resistance and the monitored load effect respectively. This concept is actually only valid when assuming normal distributions for R and M. Since the recorded sensor data can be positive or negative, it is more reasonable to calculate the associated reliability index for each sensor i:

$$\beta_i = (\mu_R - \mu_{Mi})/(\sigma^2_R + \sigma^2_{Mi})^{1/2} \tag{7}$$

where μ_{Mi} is the mean monitored load effect associated with sensor i and σ_{Mi} the standard deviation of the monitored load effect associated with sensor i. The mean monitored load effect μ_{Mi} could be considered as the mean of the recorded maximum or the maximum value during the duration of the entire monitoring process [17], [18]. However, the time duration of the monitoring should be limited to avoid the effect of time-dependent degradation effects. In this study the maximum load effect during the entire monitoring process is considered as a random variable characterized by the mean μ°_{Mi} and the standard deviation:

$$\sigma^\circ_{Mi} = \mu^\circ_{Mi} \cdot \sigma_R/\mu_R \tag{8}$$

which yields the reliability index:

$$\beta^\circ_i = (\mu_R - \mu^\circ_{Mi})/\{\sigma_R\,[1 + (\mu^\circ_{Mi}/\mu_R)^2]^{1/2}\} \tag{9}$$

As can be seen in Eq. (9), the CoV of R and M are considered equal. This is a very important and crucial/crude assumption. It can be assumed to be a conservative assumption and therefore it is acceptable in a first approach for the proposed reliability-based framework. In addition to the uncertainties in the material and loading, the uncertainties associated with the sensors e_s (%) should be included in the reliability index by using the factor

$$f_s = 1 + e_s \tag{10}$$

as follows:

$$\beta^\circ_{i,e} = (\mu_R - \mu^\circ_{Mi} \cdot f_s)/\{\sigma_R\,[1 + (\mu^\circ_{Mi}/\mu_R)^2]^{1/2}\} \tag{11}$$

In the following studies, a sensor accuracy of 1.04 has been assumed.

5 L110 bridge case study

The L110 bridge is part of a new Austrian railway line connecting St. Pölten to Vienna. The bridge has a reinforced concrete structure with three spans (19.0 – 22.0 – 19.0 m, see Fig. 6). The eastern pier of the bridge serves as a longitudinally fixed bearing. Both the piers and the abutments are founded on bored piles (d = 120 cm).

The bridge was designed in prestressed concrete with a rectangular shape (as depicted in Fig. 6). In order to be able to drain surface water, the top surface of the bridge cross-section has 2.5 % falls from the centre of the bridge to the outer edges. There are two load-distribution plates on the bridge structure, fixed on the sides of the abutments by two square "dowels" (shear connections) that are intended to constrain the plates' longitudinal displacement (relative to the bridge structure).

The track supporting layers (ÖBB-Porr system) rest on those load-distribution plates. Each of the track supporting layers is provided with eight supporting plates for the rail section. The rail fastening over the entire bridge consists of Vossloh clamps. At the transitions between the bridge and the abutments, attention has been paid to the longitudinal displacements of the bridge. As the eastern pier constitutes a fixed support for the bridge in the longitudinal direction, only the effect of a 19 m span could be observed on the eastern abutment, whereas on the western abutment it was possible to observe the effect of a 41 m longitudinal span. The metrological instrumentation focused on track 7 (since track 9 was built at a later date) at the joint between the bridge and the western abutment. The CWR sections span this transition region and the effect of the relative movement of the bridge in this zone on the rail has been reduced by the fastenings and partly by the sliding of the rail on the fastenings.

The rails are welded in sections positioned on the abutments and they are elastically supported through the track supporting layer by the non-ballasted track. Thus, the rails, through their fastening system, connect the bridge to the abutment in the longitudinal direction. The rail fasteners on the bridge have a defined, reduced yielding resistance. Therefore, the force–displacement behaviour of this interaction was mainly monitored.

6 Description of measuring system

The measurement sections are in the western abutment region where the relative movement occurs between the bridge superstructure and the abutment. In these sections the slip of the rail was measured as the differential longitudinal displacement between the lower flange (or foot) of the rail and the slab track. Furthermore, the rail strains were measured by means of inductive strain gauges. These measurement sections were located relatively close to the west abutment, and the distance intervals were chosen to increase with increasing distance from the abutment (as depicted in Fig. 7). In order to compensate for systematic errors, a tensionless "dummy" rail section was additionally instrumented. The temperature of the rail, the track supporting layer and the supporting structure were measured in preset sections. The air temperature was also recorded. Longitudinal motion of the bridge was recorded on the basis of signals from transducers that were mounted between the structure and the abutments (or piers). In the western span, the vertical accelerations of the supporting structure were recorded at one point. Two track slab layers were equipped with strain sensors during the concrete precast-

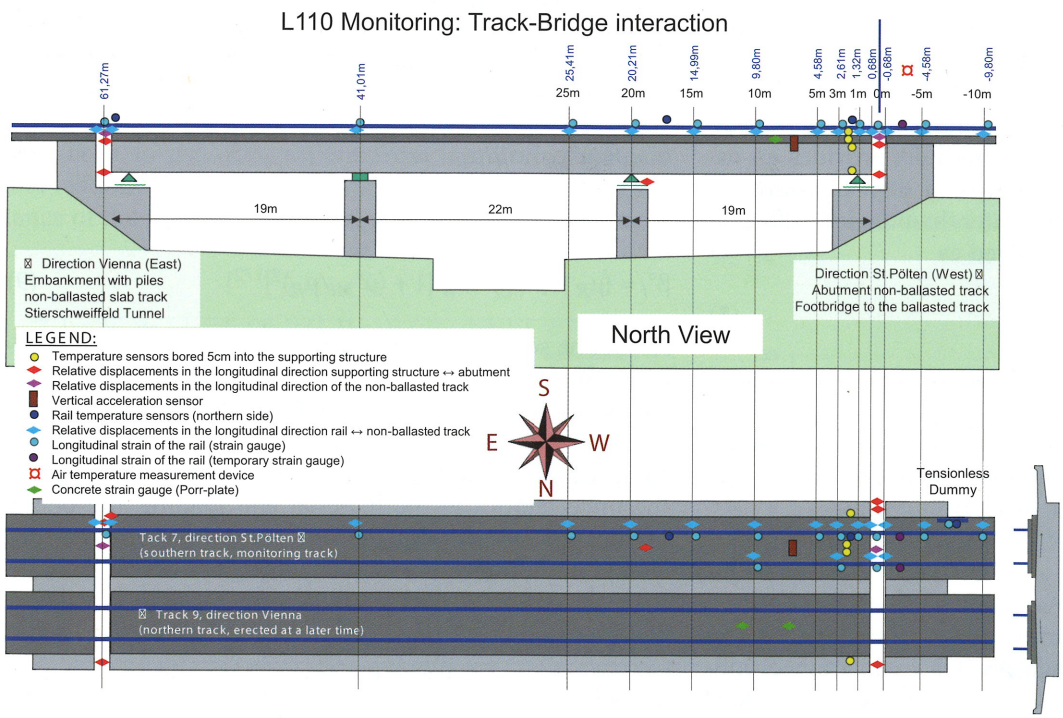

Fig. 6. Structural scheme of L110 bridge and description of monitoring system

Fig. 7. Example of measurement devices for monitoring the L110 bridge

ing and afterwards installed on the bridge. Some photos of the measuring devices used for monitoring the L110 bridge are depicted in Fig. 7.

7 A brief look at the measurements

Fig. 8 is a schematic presentation of how the temperature influences the behaviour of the bridge and the rail. As there is quite a large difference between the stiffnesses of the two, the behaviour of the bridge dominates the interaction. At positive temperature variations, the structure of the bridge elongates, thus recording positive displacements (elongation). At the same time, compression stresses develop in the rail due to the fact that it is continuously welded. Thus, the rail fastenings are subjected to the shear deformations caused by the relative longitudinal deformations between the bridge structure and the rails.

As presented in previous sections of the current paper, the fasteners are considered to possess a bilinear constitutive behaviour. Thus, as long as their behaviour remains within the elastic domain, it will be strongly influenced by the movement induced by the bridge structure.

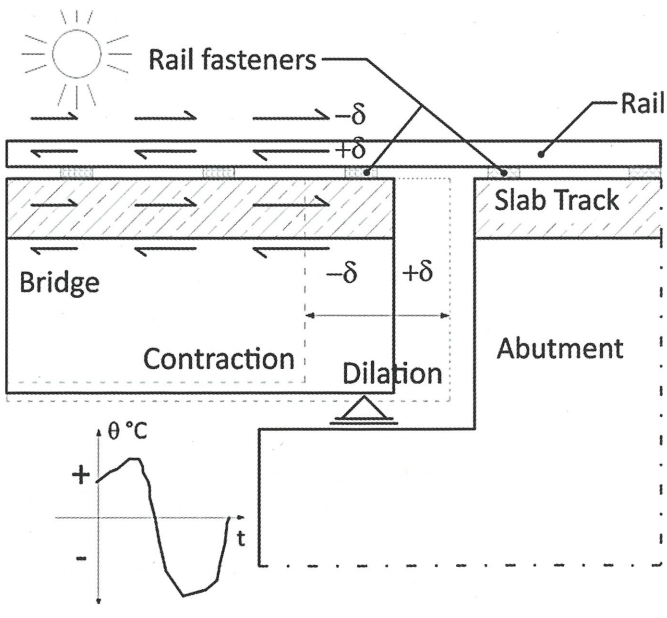

Fig. 8. Temperature influence on bridge and rail behaviour

8 Relative displacement between bridge and abutment

For instance, Fig. 9 presents the distribution of the relative displacement between the bridge and the abutment in comparison to the structure temperature (measured by a sensor that was drilled 5 cm into the bridge structure). In order to handle and process the data better, it is necessary to transfer the data from the time to the frequency do-

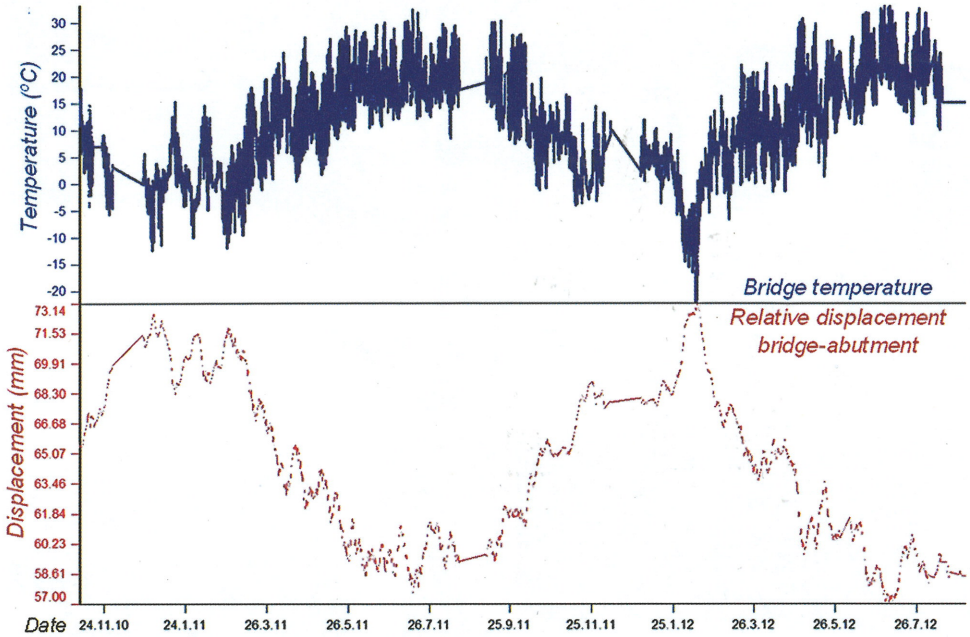

Fig. 9. Bridge temperature and bridge-abutment relative displacement variations

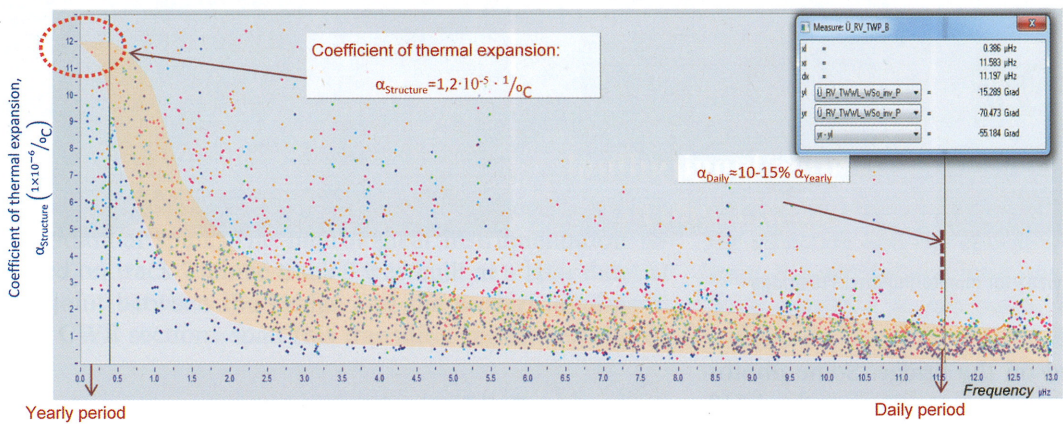

Fig. 10. Coefficient of thermal expansion for bridge structure

main. Furthermore, by dividing the relative displacement by the bridge span and relating it to the temperature it is possible to obtain the coefficient of thermal expansion α_T for the bridge structure. This is plotted in the frequency domain in Fig. 10 showing that, for the long term, the measured coefficient of thermal expansion tends to its theoretical value of 1.2×10^{-5} °C^{-1}. In the same picture it can be seen that, for the short-term behaviour (i.e. daily period), the coefficient of thermal expansion equals only 10–15 % of the long-term value. This can be explained by the environmental disturbances (caused, for example, by the traffic on road L110, the working conditions on the bridge etc.) and not by the temperature variations.

9 Rail forces induced by temperature variation

The axial force differences are plotted against the rail temperature in Fig. 11. From this diagram it is easy to see that the axial forces decrease in the rail as the temperature increases. It should be mentioned that the sign convention adopted is: plus (+) for compression (while the rail is contracting) and minus (–) for tension (while the rail is dilating).

It is easy to see the different behaviour of the rail before and after it was welded and fixed to the slab track: the gradient of the axial force variation with temperature is larger after welding (due to additional restraints) than before welding the rails. This is highlighted in Fig. 11 together with the hypothetical case in which the rail on the bridge would have been welded to the rail on the abutment and fixed to the slab track from the beginning. Fig. 12 better highlights the behaviour of the rail at the moment of its constraint through an "instantaneous" reduction in the relative displacements between the rail and the slab track.

10 Relative displacements between rail and slab track

By plotting the graph of the relative displacements between the rail and the slab track versus the temperature of the rail (see Fig. 13), it is possible to obtain the influence of the latter on the behaviour of the fastenings. The curves

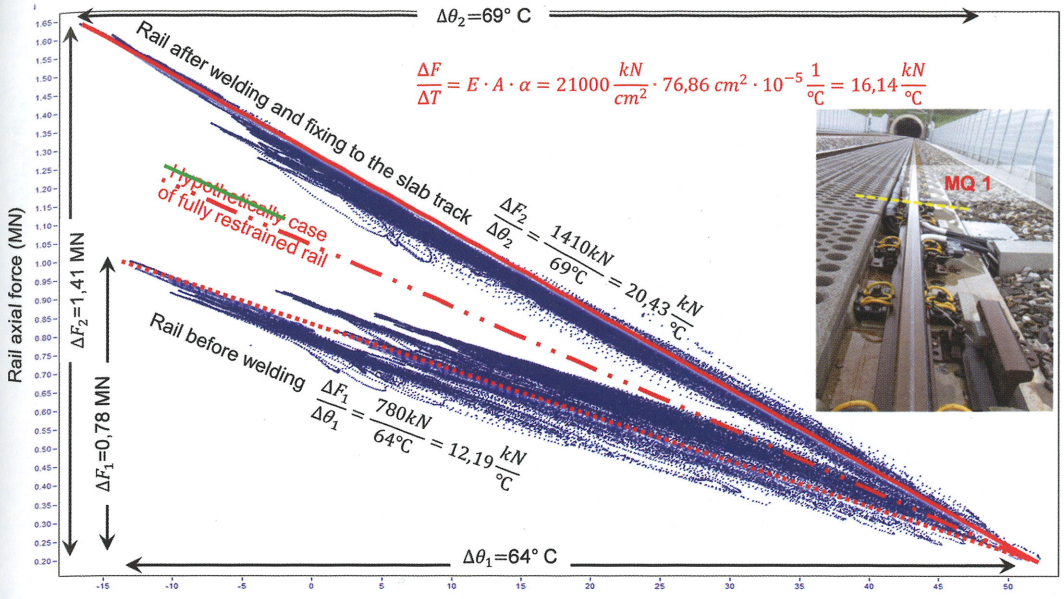

Fig. 11. Axial forces in rail in different measuring sections

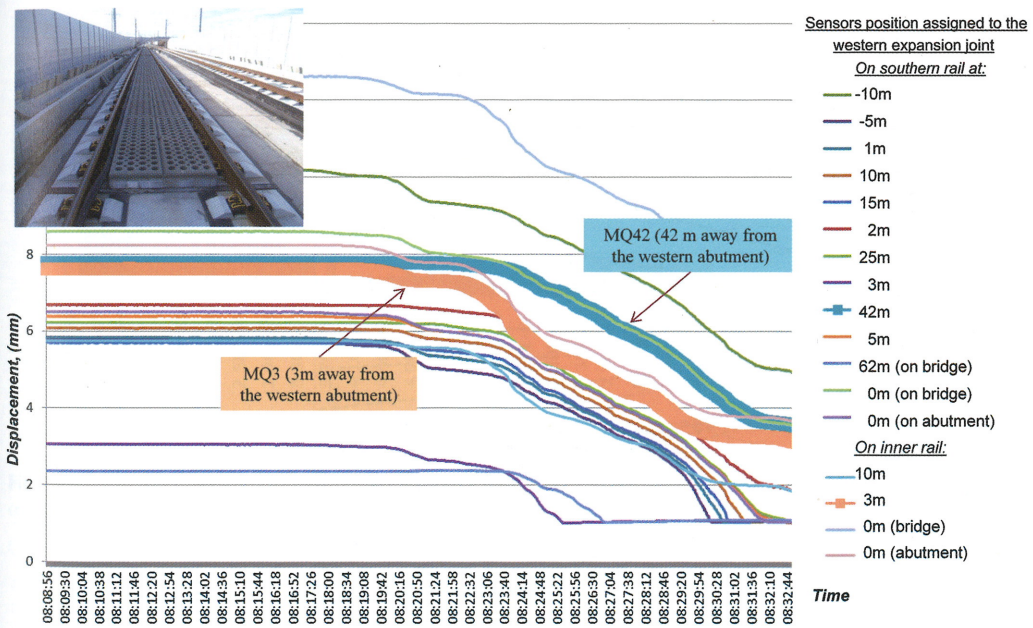

Fig. 12. Relative displacements between rail and slab track, recording the moment of welding the rail on the bridge to the rail on the abutment

plotted in Fig. 13 show the sensors recording the relative displacement between the rail and the slab track in the proximity of the joint between the bridge and the abutment on the western side (they are able to represent the relative opening of the joint between the bridge and the western abutment). The sensors represented in Fig. 13 were positioned on both sides of the joint (blue curve = on bridge, red curve = on abutment), also highlighting the influence of the latter on the relative displacement between the rail and the slab track. Both sensors exhibit a hysteretic behaviour, dependent on the temperature, with different amplitudes of the cycles (the relative displacement doubles for positive temperatures of the rail, e.g. A1/2A1 in Fig. 13).

The dashed lines in Fig. 13 represent the regression lines of the two curves. They are meant to help establish the ratios of the relative displacements along the bridge related to the opening of the joint between the bridge and the abutment (computed as the difference between the displacements recorded on both sides of the joint). The regressions were computed for all the sensors depicted by Fig. 7 and they are presented in Fig. 14.

Based on their stiffness, the bridge and the abutment exhibit different relative displacements and this fact is clearly emphasized by Fig. 14 and Fig. 15. It can be seen that in the proximity of the joint between the bridge and the abutment, the recorded relative displacements are split 40/60 %. Away from the western abutment, the influence

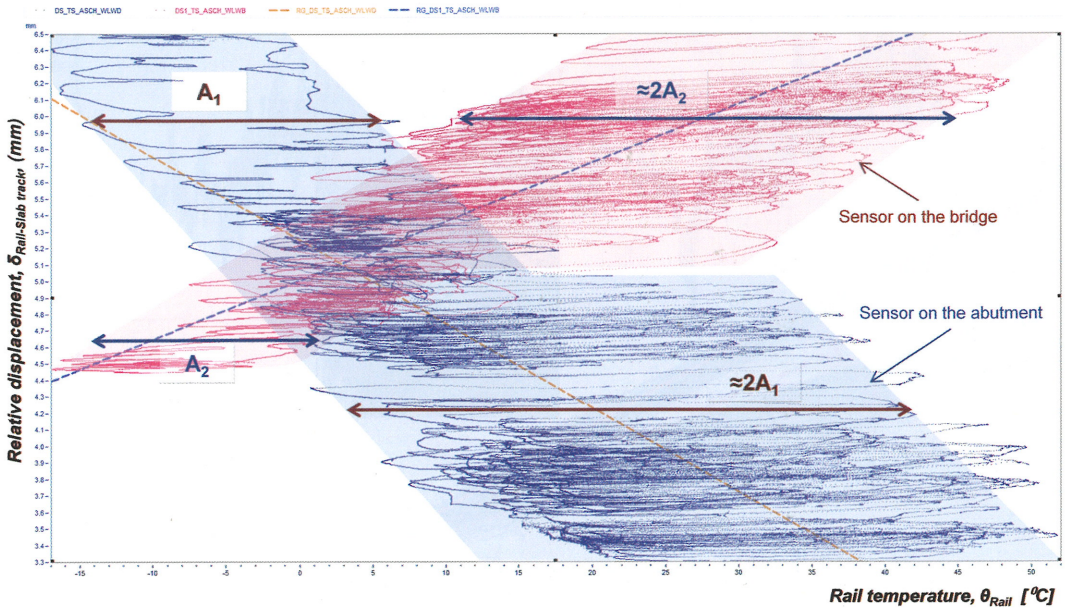

Fig. 13. Relative displacements versus rail temperature for the sensor in the proximity of the western abutment

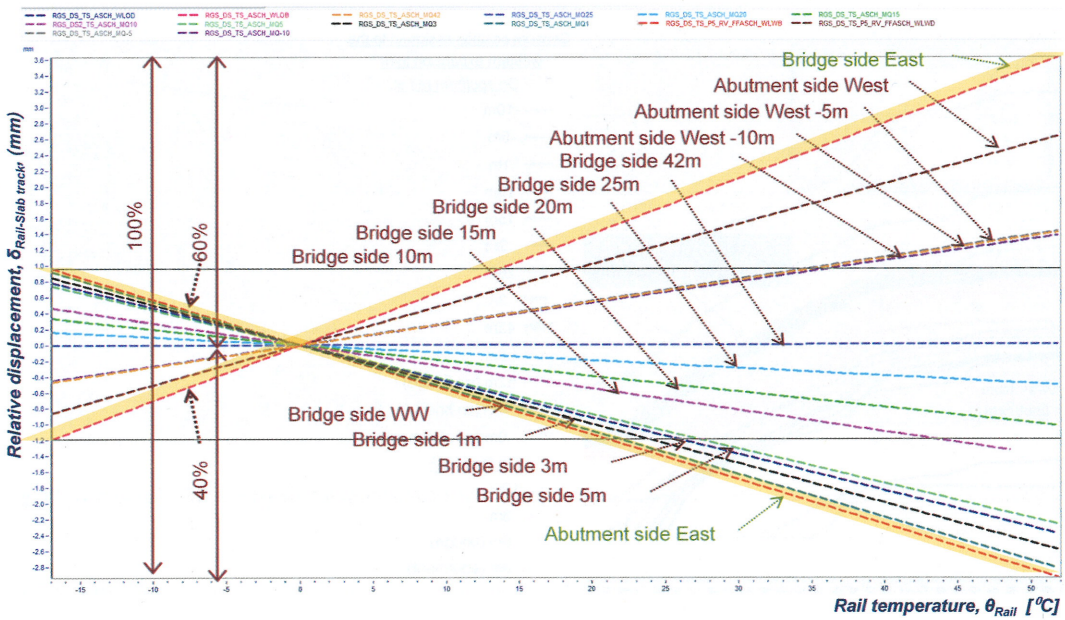

Fig. 14. Tendency of relative displacements between rail and slab track vs. the rail temperature θ_{Rail}

of the bridge on the relative displacements deceases and vanishes altogether about 25 m from the joint. This indicates that the shorter span of the bridge (the 19 m span between the eastern abutment and the pier where the bridge has a fixed support) is stiffer and thus also influences the relative displacements beyond the pier, leading to a zero relative displacement in the measurement section at 25 m from the western abutment (as depicted by Fig. 15).

11 Reliability assessment based on monitoring measurements

The structural safety requirements imposed on CWR need to be clearly defined as they can have a major influence on the extent of interventions. The monitoring of action effects on the bridge and on the rails discussed above reduces uncertainties and helps to understand the complex rail-structure interaction system. Yet, some safety margin needs to be respected, either by considering a partial safety factor or by some criterion of target level of acceptable values or thresholds as used in this study. For a realistic reconstruction of rail stresses in the critical locations above the bridge abutments, the multi-level monitoring strategy for the L110 bridge presented above has been coupled with a non-linear modelling approach [21]. There was the observation of a) the bridge longitudinal movement u_a and the temperature fields in the bridge structure (which allowed the determination of the thermal temperature coefficient for short- and long-term temperature processes, as shown in Fig. 16) and b) the rail strains or stresses due to a rail stress $L \sim 122$ N/mm^2 for $T \sim -15$ °C and $L \sim 265$ N/mm^2 for $T \sim 50$ °C, as shown in Fig. 17.

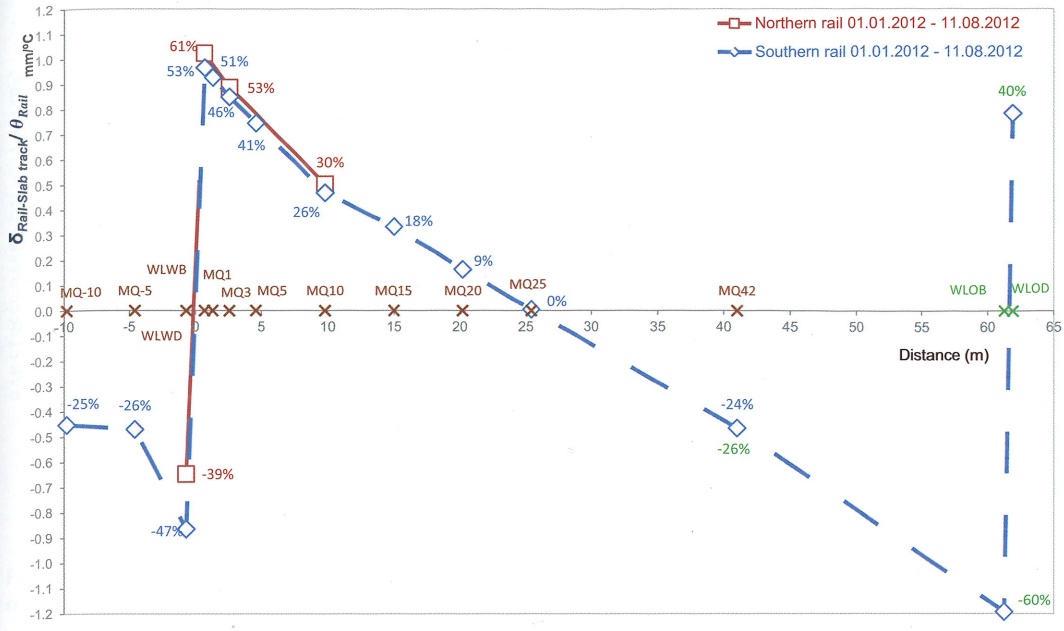

Fig. 15. Distribution of rail-slab track relative displacement with respect to rail temperature along the entire measured section

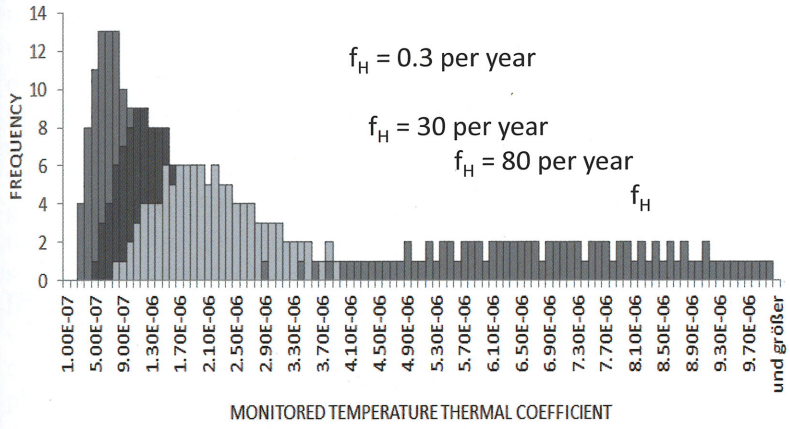

Fig. 16. Monitored coefficient of thermal expansion of bridge structure for $\alpha_{Tmean} = 8.0 \cdot 10^{-6}$ 1/C with a frequency $f_H = 0.3$ per year, $\alpha_{Tmean} = 2.2 \cdot 10^{-6}$ 1/C with $f_H = 30$ per year, $\alpha_{Tmean} = 1.0 \cdot 10^{-6}$ 1/C, with $f_H = 80$ per year, and $\alpha_{Tmean} = 0.8 \cdot 10^{-6}$ 1/C with $f_H = 115$ per year

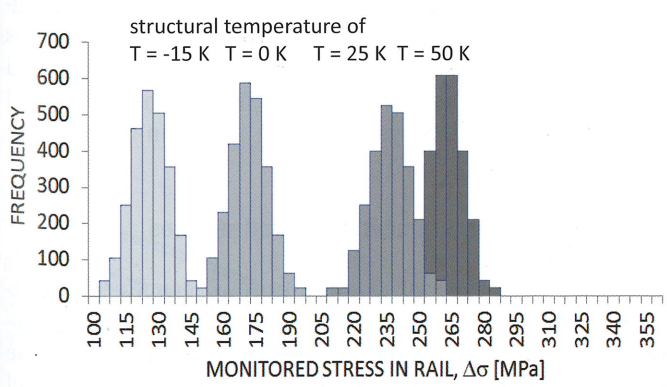

Fig. 17. Monitored rail stress above the abutment for a structure temperature of $T = 50$ K, $T = 25$ K, $T = 0$ K and $T = -15$ K

The observations from the monitoring systems and the laboratory studies of the longitudinal and shear resistance of the rail-structure interaction served for the calibration of the non-linear finite element models and modelling of the coupled system. The aim of the modelling was to verify the rail stresses caused by temperature changes in the rail and the structure. Fig. 18 portrays the bridge expansion u_a with respect to temperature changes in the structure, where short- and long-term temperature processes have been differentiated by considering the variability in the thermal temperature coefficient (according to Fig. 16).

The non-linear modelling allows, on the one hand, the monitored strains or stresses to be verified and, on the other, the verification of the longitudinal and shear stiffness of the complex rail-structure interaction model. For instance, Fig. 19a presents the rail stress distribution obtained from the complex non-linear finite element model. These distributions are verified with the monitoring systems sketched previously for selected monitored temperature loading processes.

From these curves it is possible to verify the effects of structural movements on the rail stresses, especially the uneven distributions over the supports originating from

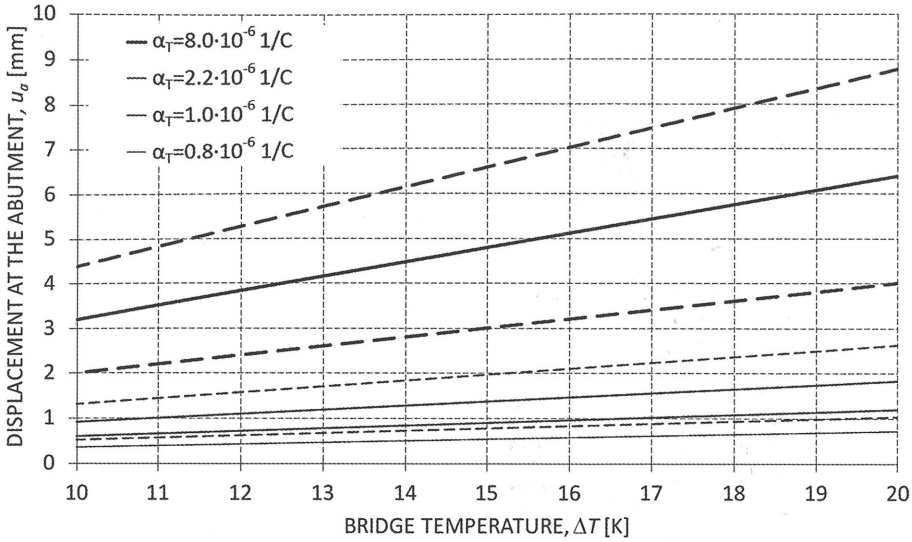

Fig. 18. Computed bridge expansion u_a based on the monitored thermal expansion coefficient for $\alpha_{Tmean} = 8.0 \cdot 10^{-6}$ 1/C with a frequency $f_H = 0.3$ per year, $\alpha_{Tmean} = 2.2 \cdot 10^{-6}$ 1/C with $f_H = 30$ per year, $\alpha_{Tmean} = 1.0 \cdot 10^{-6}$ 1/C, with $f_H = 80$ per year, and $\alpha_{Tmean} = 0.8 \cdot 10^{-6}$ 1/C with $f_H = 115$ per year

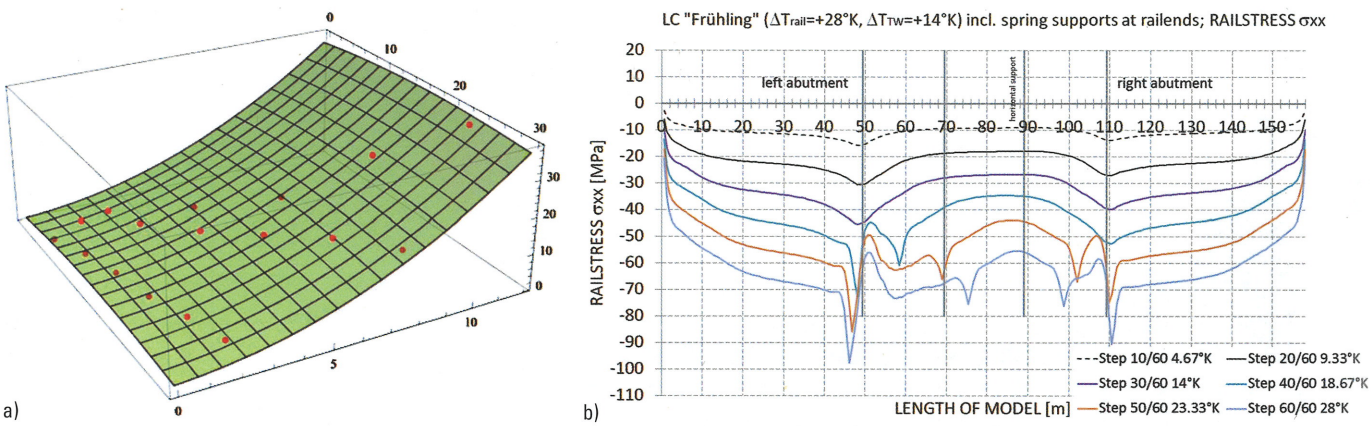

Fig. 19. Rail stress distribution obtained from non-linear finite element modelling: a) rail stress peaks $\Delta\sigma$ above the abutment vs. bridge temperature ΔT_{trag} (0 to 15 K), and vs. rail temperature ΔT_{rail} (0 to 30 K), and b) rail stress distribution in rails running over the L110 bridge for selected rail/bridge temperature combinations (step $\Delta T_{trag}/\Delta T_{rail}$ K)

the structural movements, as can be seen in Fig. 19b. These uneven stresses distributions can be described as a function of the bridge and rail temperature processes as shown in Fig. 19a for the L110 bridge. Eq. (12) represents the corresponding parabolic function and associated coefficients, which has been adjusted by the least squares method to the rail stress peaks $\Delta\sigma$ above the abutment extracted from the non-linear finite element analysis. These steps and elements are essential for the following reliability assessment of the acceptable rail stresses.

$$\sigma = \sigma_0 + a_1\,\Delta T_{trag} + a_2\,\Delta T_{trag}^2 - a_3\,\Delta T_{trag}^3 + b_1\,\Delta T_{rail} - b_2\,\Delta T_{rail}^2 + b_3\,\Delta T_{rail}^3$$

where $\sigma_0 = 2.32382$, $a_1 = -0.667091$, $a_2 = 0.0578125$, $a_3 = 0.00134827$, $b_1 = 2.54474$, $b_2 = 0.244579$, $b_3 = 0.0252026$ (12)

The functional dependence between rail stresses and the rail and structure temperatures together with the associated short- and long-term thermal coefficients discussed previously results in the rail stresses as illustrated in Fig. 20. For instance, a short-term temperature process of 15 °C in the L110 bridge causes a rail stress of 60 MPa, and a long-term process results in 20 MPa. In addition, uncertainties in the functional interrelation (see Eq. (12)) are captured by a coefficient of variation CoV = 0.09, which was derived from the monitoring systems used and non-linear finite analyses.

12 Reliability assessment for the rail stresses

The sensor readings of the monitoring systems, the non-linear analyses results and the functional relations between structure and rails derived are used to determine the stress states and, consequently, the reliability level for the structural rails monitored. For the reliability assessment, the rail stresses σ_D are multiplied by a factor $\theta = 1.08$ according to [19]. The predefined stress thresholds in DIN-Fb 101 [11] for CWR on bridges are used: $\sigma_{tension} = 112$ N/mm^2 and $\sigma_{compression} = 72/92$ N/mm^2. The standard deviation of the stresses $\sigma(\sigma_{D,T})$ is derived assuming that the coefficient of variation (CoV = 0.074) is equal to that of the yield strength [20]. The maximum ran-

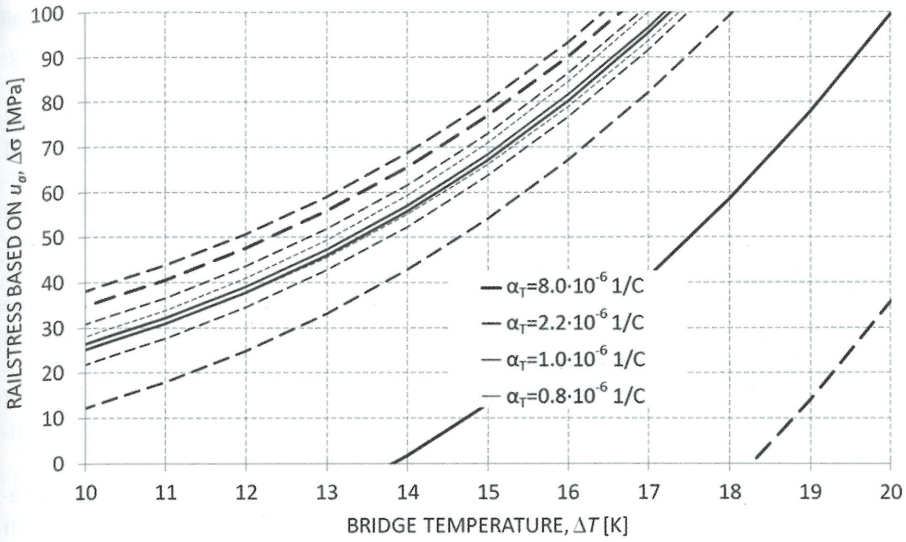

Fig. 20. Computed rail stresses above the abutment for $\alpha_{Tmean} = 8.0 \cdot 10^{-6}$ 1/C with a frequency $f_H = 0.3$ per year, $\alpha_{Tmean} = 2.2 \cdot 10^{-6}$ 1/C with $f_H = 30$ per year, $\alpha_{Tmean} = 1.0 \cdot 10^{-6}$ 1/C, with $f_H = 80$ per year, and $\alpha_{Tmean} = 0.8 \cdot 10^{-6}$ 1/C with $f_H = 115$ per year; dashed lines represent the 5 and 95 % quantiles

dom stresses due to temperature-associated track-bridge interaction (LC1), expressed by the probabilistic indicators $\mu^\circ_{Mi,LC1}$, $\sigma^\circ_{Mi,LC1}$, and the maximum random stresses due to structural bending effects (LC2), expressed by the probabilistic indicators $\mu^\circ_{Mi,LC2}$, $\sigma^\circ_{Mi,LC2}$, are always considered in the following reliability assessment. It is essential to consider the bending of the bridge, since bending generates a vertical deflection and a rotation of the structure next to the abutments and, consequently, additional stresses in the rails. For the reliability assessment of the rail members monitored above the abutment, the mean values of the maximum random stresses resulting from the combination of load cases LC1 and LC2 have to be computed as

$$\mu^\circ_{Mi(1)} = \mu^\circ_{Mi,LC1} + \mu^\circ_{Mi,LC2} \tag{13}$$

and the standard deviation as

$$\sigma^\circ_{Mi(1)} = [(\sigma^\circ_{Mi,LC1})^2 + (\sigma^\circ_{Mi,LC2})^2]^{1/2} \tag{14}$$

Considering the same coefficient of variation (CoV = v = σ_R/μ_R = 0.074) for the maximum stresses associated with all load cases yields

$$\sigma^\circ_{Mi(1)} = v\,[(\mu^\circ_{Mi,LC1})^2 + (\mu^\circ_{Mi,LC2})^2]^{1/2} \tag{15}$$

and therefore

$$\sigma^\circ_{Mi(1)} = \sigma^\circ_{Mi,LC1}\,[1 + (\mu^\circ_{Mi,LC2}/\mu^\circ_{Mi,LC1})^2]^{1/2} \tag{16}$$

As mentioned previously, the crucial/crude assumption of an equal COV can be assumed as conservative and ac-

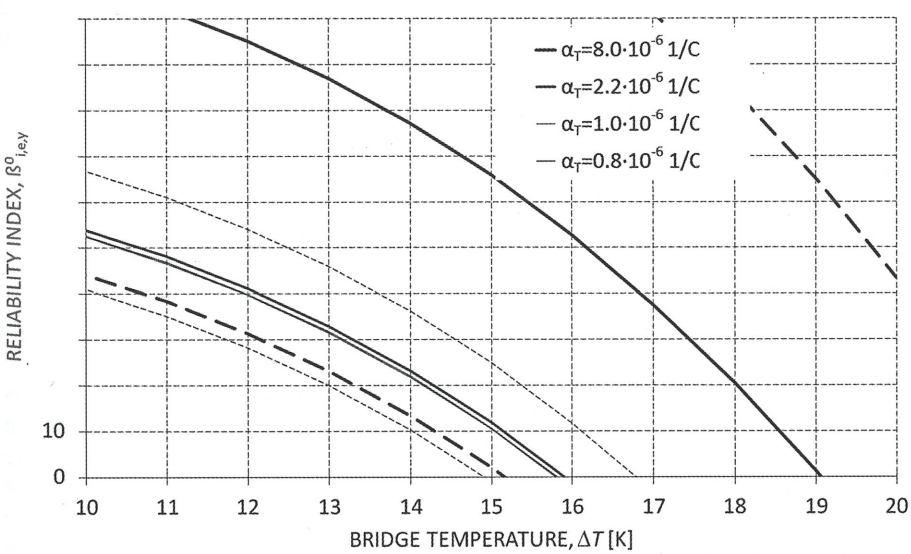

Fig. 21. Monitoring- and NL analyses-based reliability index β plotted with respect to the acceptable stress threshold of 72 MPa for $\alpha_{Tmean} = 8.0 \cdot 10^{-6}$ 1/C with a frequency $f_H = 0.3$ per year, $\alpha_{Tmean} = 2.2 \cdot 10^{-6}$ 1/C with $f_H = 30$ per year, $\alpha_{Tmean} = 1.0 \cdot 10^{-6}$ 1/C, with $f_H = 80$ per year, and $\alpha_{Tmean} = 0.8 \cdot 10^{-6}$ 1/C with $f_H = 115$ per year; dashed lines represent β with respect to the 5 and 95 % quantiles of the associated thresholds

ceptable for a first approach. Finally, the reliability index $\beta^{\circ}_{i,e,y}$ of a sensor i (y indicates the threshold for the rail stresses) can be calculated using Eq. (17) as follows:

$$\beta^{\circ}_{i,e,y} = (\mu_R - \mu^{\circ}_{Mi(1)} \cdot f_s)/[\sigma^2_R + (\sigma^{\circ}_{Mi(1)})^2]^{1/2} \quad (17)$$

The consideration of a sensor error e_s = 4 % will result in an approx. 6 % reduction in $\beta^{\circ}_{i,e,y}$.

Including the mean values of the maximum random stresses of load tests (load case LC3, such as effects of local axle loads next to the cross sections investigated, expressed by the probabilistic indicators $\mu^{\circ}_{Mi,LC3}$ and $\sigma^{\circ}_{Mi,LC3}$) in the reliability assessment requires the mean values of the maximum random stresses associated with LC1, LC2 and LC3 to be combined as follows:

$$\mu^{\circ}_{Mi(2)} = \mu^{\circ}_{Mi,LC1} + \mu^{\circ}_{Mi,LC2} + \mu^{\circ}_{Mi,LC3} \quad (18)$$

and the computation of the standard deviation:

$$\sigma^{\circ}_{Mi} = \sigma^{\circ}_{Mi,LC1} [1 + (\mu^{\circ}_{Mi,LC2}/\mu^{\circ}_{Mi,LC1})^2 + (\mu^{\circ}_{Mi,LC3}/\mu^{\circ}_{Mi,LC1})^2]^{1/2} \quad (19)$$

Fig. 21 shows the variation in the reliability index $\beta^{\circ}_{i,e,y}$ for the monitored and numerical rail stresses above the abutment on the basis of Eqs. (18) and (19). These observations were made with respect to the different thermal expansion coefficients for short- and long-term effects, as already discussed for u_a.

As can be seen from the graphs, there is a critical development of $\beta^{\circ}_{i,e,y}$ (e.g. < 5) for the L110 bridge for a temperature difference > 19 °C for long-term and > 14.5 °C for short-term temperature processes with respect to the threshold $\mu_{\sigma,compression}$ = 72/92 N/mm² (CoV = 0.074). These considerations concerning the variable thermal expansion coefficients can be mapped to a generalized concept, e.g. based on geometrical quantities such as longitudinal displacements.

13 Conclusions

This paper presents an approach for using monitoring data for the reliability assessment of structural systems with respect to track-bridge interaction and rail stress limit states. The proposed approach was used in conjunction with the L110 bridge, a structure located in Lower Austria and monitored by FCP Consult Austria. This investigation allows the following conclusions to be drawn:

1. The approach proposed allowed the probabilistic assessment of the track-bridge interaction and rail stress performance of the L110 bridge at different points in time based on real data. The reliability assessment of the rail-ridge interaction showed that according to the assumptions and thresholds described, the reliability of rail stresses not exceeding the given thresholds is given by far.
2. The non-linear finite element analyses and the monitoring of the rails running over the whole bridge also revealed that the rail sections above the abutment are the elements with the lowest reliability.
3. For long-term temperature processes involving a 15° temperature rise acting on the L110 bridge (40 m free extension length), a stress increase of max. 70 MPa occurs, and 30 MPa for short-term processes, which is significantly lower than in code specifications.
4. The monitoring systems allowed the unambiguous identification of the coefficient of thermal expansion of the concrete bridge a) for long-term and b) for short-term temperature processes. It should be noted that the thermal expansion coefficient is independent of any circumstance or temperature variation. A variable thermal expansion factor approach implies that surface temperature differs from internal temperature. In this article, an equivalent effective expansion coefficient approach is pursued in order to grasp the uncertainties of rail stresses or deformations associated with the expansion-relevant structure temperature.
5. The monitoring system also allowed the characterization of the active zones of the movement of the rails in the abutment regions and their non-linear rapid decay
6. A reliability-based non-linear finite element analysis combined with the multi-level monitoring systems revealed the non-linear character of the system and presented a lower stress distribution along the rails compared with the code specifications. There is a requirement to continue with the research, aiming to improve codes and obtain less conservative rules.
7. From the preceding analytical and monitoring-based considerations it can be deduced that the rail stress restrictions are not exceeded greatly by bridges with a free extension length of 40 m like the L110 bridge. Free expansion lengths of up to 80 m could be quite feasible, taking into account probability-based approaches.
8. New monitoring- and non-linear finite element-based engineering methods and technologies have been successfully applied to full-scale structures and their effectiveness – also in view of more sustainable concrete structures – has been demonstrated.
9. As the methods demonstrated in this research provide support for avoiding the use of expansion devices and, consequently, LCC issues, they ensure cost-savings in maintenance measures. The findings can also be used in a revision process for the current standard specifications.

Acknowledgements

The support by grants from the Austrian Research Promotion Agency within the scope of the "Shear-normal force optimization of prestressed precast concrete components (MAGIT)" project is gratefully acknowledged. The support of the National Science Foundation through Grants "Verkehrs Infrastruktur Forschung" of FFG, OEBB and BMfVIT to University of Natural Resources and Life Sciences is also gratefully acknowledged. The opinions and conclusions presented in this paper are those of the writers and do not necessarily reflect the views of the sponsoring organizations. The writers wish to express their profound thanks to Dr. *Hannes Kari* and Dr. *Thomas Petraschek* from ÖBB for their constructive comments and suggestions and access to the data. Many of their comments and suggestions have served to improve this paper.

References

1. *Göbel, C.*, 1999. Ausbau und Instandhaltung bestehender Eisenbahnstrecken. EI Eisenbahningenieur 50, 6.
2. ZOV 55, 2001. Zusatzbestimmungen zu Oberbauvorschrift der ÖBB: Lückenlose Gleise und verschweißte Weichen.
3. *Ruge, P., Trinks, C., Muncke, M., Schmälzlin, G.*, 2004. Längskraftbeanspruchung von durchgehend geschweißten Schienen auf Brücken für Lastkombinationen. Bautech. 81, 537–548.
4. *Ruge, P., Birk, C.*, 2007. Longitudinal forces in continuously welded rails on bridgedecks due to nonlinear track-bridge interaction. Comput. Struct. 85, 458–475.
5. *Ruge, P., Widarda, D., Birk,* C., 2007. Longitudinal track-bridge interaction for loadsequences. Track-Bridge Interact. High-Speed Railw. Workshop, 93–116.
6. *Widarda, D. R.*, 2008. Longitudinal forces in continuously welded rails due to nonlinear track-bridge interaction for loading sequences.
7. European Committee for Standardization (CEN), 2003. Eurocode 1, Part 2 (EN 1991- 2). Actions on Structures; Traffic loads on bridges.
8. *Kerr, A. D.*, 1978. Analysis of thermal track buckling in the lateral plane. Acta Mech. 30, 17–50.
9. *Kerr, A. D.*, 1980. An improved analysis for thermal track buckling. Int J. Non-Linear Mech. 15, 99–114.
10. *Lim, N.-H., Park, N.-H., Kang, Y.-J.*, 2003. Stability of continuous welded rail track. Comput. Struct. 81, 2219–2236.
11. DIN, 2003. DIN-Fachbericht 101. Einwirkungen auf Brücken.
12. UIC (Union Internationale des Chemins de fer), 2001. Track/bridge interaction. Recommendations for calculations.
13. *Schneider, K.-J.*, 2002. Bautabellen für Ingenieure, Volume 15. ed. Werner Verlag.
14. *Frangopol, D. M., Strauss, A., Kim, S.*, 2008a. Bridge reliability assessment based on monitoring. J. Bridge Eng. 13, 258–270.
15. *Shinozuka, M.*, 1983. Basic analysis of structural safety. J. Struct. Eng. 1093, 721–740.
16. *Estes, A. C., Frangopol, D. M.*, 1998. RELSYS: A computer program for structural system reliability analysis. Struct. Eng. Mech. 68, 901–919.
17. *Strauss, A., Frangopol, D. M., Kim, S.*, 2008. Use of monitoring extreme data for the performance prediction of structures: Bayesian updating. Eng. Struct. 30, 3654–3666.
18. *Frangopol, D.M., Strauss, A., Kim, S.*, 2008b. Use of monitoring extreme data for the performance prediction of structures: General approach. Eng. Struct. 30, 3644–3653.
19. JCSS, 2001. JCSS probabilistic model code; Part I. Basis of design.
20. *Strauss, A., Kala, Z., Bergmeister, K., Hoffmann, S., Novák, D.*, 2006a. Technologische Eigenschaften von Stählen im europäischen Vergleich. Stahlbau 751, 55–60.
21. *Strauss, A., Mordini, A., Bergmeister, K.*, 2006b. Nonlinear finite element analysis of reinforced concrete corbels at both deterministic and probabilistic levels. Comput. Concr. 3, 123–144.

Alfred Strauss
Associate Professor
Department of Civil Engineering & Natural Hazards
University of Natural Resources & Life Sciences
Vienna, A-1190, Austria
alfred.strauss@boku.ac.at

Saeed Karimi
Associate Researcher
Department of Civil Engineering & Natural Hazards
University of Natural Resources & Life Sciences
Vienna, A-1190, Austria
saeed.karimi@boku.ac.at
(corresponding author)

Dr. Eng. Fritz Kopf
FCP – Fritsch, Chiari & Partner ZT GmbH
Vienna, A-1140, Austria
kopf@fcp.at

Dr. Eng. Catalin Capraru
FCP – Fritsch, Chiari & Partner ZT GmbH
Vienna, A-1140, Austria
capraru@fcp.at

Konrad Bergmeister
Professor
Department of Civil Engineering & Natural Hazards
University of Natural Resources & Life Sciences
Vienna, A-1190, Austria
konrad.bergmeister@boku.ac.at